Antibacterial titanium dioxide coatings for CoCrMo orthopaedic implants

Agnese D'Agostino [a,b,*], Michele Bertolini [a], Nina Bono [a], Matteo Pavarini [a], Paolo Tarsini [a], Gabriele Candiani [a,b], Luigi De Nardo [a,b], Roberto Chiesa [a,b]

[a] *Department of Chemistry, Materials and Chemical Engineering "G. Natta" Politecnico di Milano, Milan, Italy* [b] *National Interuniversity Consortium of Materials Science and Technology (INSTM), Florence, Italy*

doi: 10.1016/j.apsusc.2022.155300

Keywords:
CoCrMo alloys
Titanium dioxide
Silver
Gallium
Antibacterial coatings

Abstract:
Periprosthetic joint infections (PJIs) still remain a severe complication after arthroplasty despite the significant advances in manufacturing materials in the orthopaedic field. The sol–gel based coating strategy is attracting interest for its multifaceted potential to design surfaces capable of exerting antibacterial properties. In this study, the sol–gel technique is employed to obtain a new class of titanium dioxide coatings doped with silver and gallium ions to minimize the adhesion and bacterial colonization on the CoCrMo surfaces. Uniform anatase titania coatings with hydrophobic behaviour and nanometer thickness (50–200 nm) were obtained by dipping CoCrMo samples in TiO_2 sols with different compositions. The physicochemical characterization of coatings using EDS, GDOES, and ICP-OES confirmed the incorporation of doping agents. Antimicrobial assays were performed against Gram-positive *S. aureus* and Gram-negative *E. coli* bacteria, demonstrating a satisfying antibacterial activity. Furthermore, all the coatings tested showed no cytotoxicity and osteodifferentiation potential. Thus, the herein sol–gel strategy could represent a powerful tool for surface modification of CoCrMo-based materials for implantable devices.

1. Introduction

Metallic materials are widely used to manufacture medical devices for several applications. Notably, the outstanding properties of Cobalt-Chromium-Molybdenum (CoCrMo) alloys, such as high stiffness and superior wear resistance of bearing surfaces, have spurred such material in the manufacturing of components for knee and hip arthroplasty [1]. CoCrMo alloy described within the ISO 5832–12 standard remains one of the best choices for bearing surfaces because of its superior wear resistance and processability (grinding and polishing compatibility) and its proven clinical history. Interestingly, the well-established corrosion and wear resistance of CoCrMo alloy is owed to a strong, thin chromium oxide passive layer that spontaneously forms on the metallic surface, making the material protected from the corrosion process. Considering that the use of medical devices has grown significantly in recent years, it is necessary to ensure their performance, safety and quality by strict regulatory frameworks [2]. The employment of CoCrMo alloys in medical devices is strongly supported since the exposure to these materials does not represent a hazard for toxicity (polycythemia, thyroid changes, or myocardial damage); carcinogenicity or reproductive toxicity [3–5]. According to these motivations, CoCrMo based materials can provide health and safe benefits to patients.

Despite the advances in the manufacture of materials to be used in the orthopaedic field, periprosthetic joint infections (PJIs) still remain a serious complication after arthroplasty. Even though there is still no universal delineation of PJIs, this kind of infection frequently arises during hospitalization and it is attributed to endogenous skin flora or exogenous sources from the operating theatre [6]. The surfaces of prosthetic devices are susceptible to bacterial colonization, which may lead to biofilm formation and severe septic disease [7,8]. *Staphylococcus aureus* (*S. aureus*) and *Staphylococcus epidermidis (S. epidermidis)* are the primary pathogens responsible for orthopaedic implant infections. Epidemiological studies have shown an infection rate close to 1 % for hip replacement, to 2 % for knee replacement and even to 9 % for elbow replacement [9]. Although significant progress has been made in pre- and *peri*-operative procedures, as well as in post-operative care, there has been no significant reduction in the rate of infection in the last two decades. Joint *endo*-prostheses are long-term implanted devices, and their materials and surfaces must meet high requirements in terms of biocompatibility while preventing any adverse reaction of the surrounding tissues. In view of these overall considerations, the surface implant should prevent bacterial adhesion, proliferation and colonization whilst should promote proper tissue reactions, such as osteointegration or soft tissue physiological response.

Several prevention approaches have been developed so far to mitigate the risk of infection in implant surgery. One possible strategy to reduce the incidence of infections and prevent significant patient complications is to develop material surfaces that intrinsically inhibit bacterial adhesion and growth, and the development of biofilm. Thus, many different techniques have been envisioned to modify the surfaces of biomaterials with the aim of reducing bacterial growth and biofilm formation. Proper morphological modification, as well as chemical or physical surface functionalization and antimicrobial agents immobilization, were studied and considered [10]. Ideally, such surface modifications should bring a twofold benefit to orthopaedic implants: (i) improve tissue interactions, such as osteointegration; (ii) prevent bacteria adhesion and proliferation.

Currently, the sol–gel technique provides an intriguing way to modify the surface of materials because it allows to obtaining protective and functional coatings, preserving the properties of the bulk [11]. In the sol–gel synthesis two main reactions are involved: (i) controlled hydrolysis and condensation of the precursor (metal alkoxides or organic/inorganic salts) in the acidic or in basic mediums to form a colloidal solution (sol); (ii) formation of a rigid and interconnected three dimensional network (gel) *via* polycondensation by evaporation of the solvent. Subsequently, a drying process and an appropriate heat treatment are performed to obtain the desired product. Thanks to the possible processing temperatures, low costs, and the large availability of precursors, coatings with a wide range of compositions can be achieved [12]. Among the plethora of materials that are possible to prepare through sol–gel syntheses, titanium dioxide (TiO_2) nanostructures, both in the form of nanoparticles and coatings, play an important role owing to their unique photocatalytic properties, high chemical stability, low toxicity, and excellent biocompatibility [13]. TiO_2 coatings have been successfully employed in the orthopaedic field and dentistry [14]. Furthermore, *in vivo* and *in vitro* investigations have reported not only the antibacterial activity of TiO_2 but also its ability to promote osteogenic differentiation [15]. Hence, modification of implant surfaces by TiO_2 nanostructures could represent a new opportunity.

A possible method to provide CoCrMo alloys with antimicrobial properties is to develop coatings integrating cations with well-known antibacterial behaviour [16,17], such as silver (Ag) [18,19], copper (Cu) [20], zinc [20,21] and gallium (Ga) [22–24]. Among them, Ag has aroused lively interest in

the biomedical field as well as some applications have reached the maturity for clinical use [25,26]. The renowned antibacterial activity of Ag, although the working mechanisms are not fully known, is attributed to the interaction between the positive charge of the Ag ions and the anionicity of the cell membrane and DNA structure of bacteria [27]. In addition to Ag, recent studies indicated that Ga possesses bactericidal properties thanks to its capability of inhibiting biofilm formation [24] owing to its ability to mimic the iron's action in several mechanisms in bacteria metabolism [28].

Considering these premises, the biocompatibility of the TiO_2 anatase phase coupled with the antibacterial action of silver ions (Ag^+) and gallium ions (Ga^{3+}) was exploited to obtain a novel family of coatings for CoCrMo-based material implants. The preparation of doped TiO_2 coatings was carried out by combining sol–gel strategy and dipping method, choosing silver nitrate ($AgNO_3$) and gallium nitrate ($Ga(NO_3)_3$) as sources for Ag^+ and Ga^{3+}, respectively. Physico-chemical properties of TiO_2 coatings were widely investigated using (i) X-ray analyses, confirming the predominant presence of only anatase phase, (ii) water contact angle (WCA) measures, displaying hydrophobic behaviour compared to uncoated samples, (iii) evaluation of roughness parameters (Ra, Rq, Rsk, Rk), revealing that the herein surface modification approach did not significantly modify surface roughness; Scanning Electron Microscopy (SEM) highlighting homogeneous covering of the coating; Glow Discharge Optical Spectroscopy (GDOES) and Energy Dispersion Spectroscopy (EDS) demonstrated the incorporation of doping agents within the coating. Antimicrobial assays were performed against the *S. aureus* and *Escherichia coli* (*E. coli*) bacterial strains, demonstrating excellent antibacterial activity. Furthermore, all the coatings tested showed no cytotoxicity and osteodifferentiation potential. Thus, the herein sol–gel strategy could represent a powerful tool for surface modification of implantable devices.

2. Experimental

Titanium tetraisopropoxide (TTIP; purity ≥ 97 %), formic acid (purity ≥ 95 %), nitric acid (purity ≥ 65 %), Ag nitrate ($AgNO_3$; purity > 99.8 %), Ga nitrate monohydrate ($Ga(NO_3)_3*H_2O$; purity > 99.8 %) were all supplied by Merck Italy - Sigma-Aldrich. Reagents were used as received. Distilled water was employed for synthesis. Cylindrical disks of CoCrMo alloy (ISO 5832–12) with a diameter of 16 mm (**Fig. S1**) were machined by bar turning. Samples have a good geometry to facilitate subsequent *in vitro* biological testing. The surface of interest, corresponding to the bottom of the well, was previously sandblasted with synthetic alumina. *2.1. Synthesis of TiO_2 sol*

Briefly, in a glass flask, equipped with a magnetic stir bar, 4.2 mL of TTIP was added to 4.0 mL of formic acid under vigorous stirring. Then, the acidified water (90.0 mL of distilled water with 4.8 mL of nitric acid) was added. After 30 min, a homogeneous and stable solution with a clear appearance was obtained. TiO_2 doped sol was prepared by adding the proper quantity of $AgNO_3$, with a final concentration of 0.01 M (plus Ag) sol, or $Ga(NO_3)_3*H_2O$ with a final concentration of 0.01 M (plus Ga) sol, or $AgNO_3$ and $Ga(NO_3)_3*H_2O$ with a final concentration of 0.01 M for both salts plus (Ag + Ga) sol.

2.2. Dip-coating of CoCrMo disks

The dip-coating method was chosen to coat the CoCrMo disks. Samples were immersed in the solution and then extracted at a 100 mm/ min constant speed. For samples with 3 layers, treatment at 100 °C for 15 min was carried out between one deposition and another to consolidate the coating and prevent it from being washed away by the subsequent immersion. The next phase involved drying and compacting the gel: after a short drying time (5 min) in the air, samples were placed in the oven at 120 °C for 3 h. The temperature was chosen to guarantee full drying. TiO_2 coated CoCrMo samples were tagged TYPE I (plus Ag), TYPE II (plus Ga), TYPE III (plus Ag + Ga).

2.3. Physicochemical characterisation

X-ray powder diffraction (XRD) was carried out to characterise the microstructure of titanium dioxide. Small quantities of powder obtained after complete evaporation of sol and thermally treated at 120 °C were examined by Philips PW 1830, equipped with a Bragg Brentano diffractometer and Cu-Kα1 radiation (wavelength: 0.154056 nm).

Water Contact Angle (WCA) was conducted using the "sessile drop" method (*Allied Vision Technologies*), to determine the wettability of coated and uncoated CoCrMo surfaces. Measurements were carried out on the back of the CoCrMo sample, which had previously been properly polished, to avoid measurement interference due to sandblasting- induced surface roughness. 5 measurements per sample were taken, namely control sample, 1 layer sample and 3 layers sample. The obtained images were then processed with the proper software, which allowed us to extract the contact angle values.

The evaluation of roughness of uncoated samples, 1 layer samples and 3 layers sample samples was determined through a UBM Microfocus instrument considering the following parameters: Ra, Rq, Rsk, Rk (n = 3 tests per condition).

Glow Discharge Optical Emission Spectroscopy (GD-OES) was employed in order to evaluate the concentration profiles. This analysis was assessed on the polished backside surface of the samples in the case of single and 3 superimposed layers, by using a GDA 750 HR spectrometer (Spectruma, Germany).

Inductively coupled plasma optical emission spectroscopy (ICP-OES) analysis was used to detect the total concentration of antibacterial agents in the coating expressed in mg and surface density ($\mu g \times cm^{-2}$). One sample for each typology was mineralised by acid etching: two times with hydrofluoric acid and one time with hydrofluoric acid and nitric acid. The resulting solution was then analysed by Perkin Elmer Optima 8300 spectrometer.

2.4. In vitro biological characterisation

2.4.1. Antibacterial tests

Antibacterial tests were performed according to the ISO 22196:2011 (E) standard, with slight modifications [29]. Before use, uncoated (control, CTRL) and TiO_2-coated CoCrMo 1 layer samples: (plus Ag, TYPE I; plus Ga TYPE II, plus (Ag + Ga), TYPE III) were first washed with pure ethanol (EtOH), then soaked in EtOH for 1 h to be sanitised and allowed to dry overnight in a biosafety cabinet.

S. aureus DSM 346 (Gram-positive bacteria, biological safety level 2, Leibniz Institute DSMZ, German Collection of Microorganisms and Cell Cultures, Germany) and *E. coli* JM109 (Gram-negative bacteria, biological safety level 1, Leibniz Institute DSMZ) were pre-cultured overnight at 37 °C in 5 mL of nutrient broth (NB) and Luria-Bertani (LB) broth, respectively. Bacteria were kept under shaking at 130 rpm, until reaching an optical density (OD_{600nm}) of ≈0.6, corresponding to ≈10^8 bacteria/mL. The bacterial suspensions were diluted to a ≈concentration of 2 × 10^4 bacteria/mL.

Afterwards, 200 μL of each the bacterial suspension were inoculated onto each sample (n = 3 samples per material) and incubated at 37 °C for 24 h.

Bacteria cultured onto uncoated CoCrMo specimens were used as a positive control for bacterial growth (CTRL).

For each material (coating), the antibacterial efficacy was evaluated using the turbidity method (i.e., OD_{600nm} measurements) [29]. Briefly, 24 h post-inoculum, bacterial suspensions were recovered and transferred into a 96-well plate, and the OD_{600nm} of each well was read using a GENios Plus reader. The antibacterial efficiency was calculated according to Eq. (1):

$$\text{antibacterial activity (\%)} = 1 - \left[- OD_{600nm,\ sample}/OD_{600nm,\ CTRL} \right] \times 100 \quad (1)$$

2.4.2. Indirect cytotoxicity tests

Indirect cytotoxicity tests were performed according to the ISO 10993–5:2009 norm. Cell culture medium (Dulbecco's Modified Eagle Medium (DMEM)) supplemented with 1 mM sodium pyruvate, 10 mM HEPES buffer, 100 U/mL penicillin, 0.1 mg/mL streptomycin, 2 mM glutamine and supplemented with 10 % (v/v) fetal bovine serum (FBS) (hereafter referred to as complete medium) was used as extraction vehicle. Briefly, (CTRL, TYPE I, TYPE III samples) (n = 4 per sample) were prepared as described herein above and placed into separate wells of 12-well plates inoculated with a 300 μL complete medium of each. Following incubation in standard culture conditions (37 °C in a humidified atmosphere under a constant supply of 5 % CO_2) for 24 or 72 h, sample eluates were collected and stored at T = -80 °C until use.

Mycoplasma-free MG63 cells (human osteosarcoma cell line cells; American Type Culture Collection, ATCC, VA, USA) were seeded in 96- well culture plates at a density of 10^4 cells/well in 100 μL of complete medium and incubated in standard culture conditions for 24 h. Afterwards, the medium was replaced with 100 μL/well of eluates (n = 3 per time point), and then cells were incubated for further 24 h in standard culture conditions. Cells cultured in a complete medium were used as negative controls of cytotoxicity (CTRL, n = 4). Twenty-four hours post- incubation, cell viability was assessed using a resazurin assay (Merck).

Briefly, the culture medium was discarded, and each well was filled with 100 μL of complete medium containing 10 μL of resazurin dye solution. Cells were incubated in standard culture conditions for 2 hrs, and then the fluorescence (λ_{ex} = 540 nm; λ_{em} = 595 nm) was read using a Synergy H1 microplate reader (BioTek, Italy). Viability of CTRL cells was assigned as 100 %. For each well, cell viability was calculated according to Eq. (2):

$$\text{viability (\%)} = [RFU_{cells}/RFU_{CTRL}] \times 100 \quad (2)$$

2.4.3. Alkaline phosphatase (ALP) assay

Mycoplasma-free SAOS-2 cells (human osteogenic sarcoma cell line, HTB-85; ATCC) were cultured in McCoy culture medium supplemented with 1 mM sodium pyruvate, 100 U/mL penicillin, 0.1 mg/mL streptomycin, and 2 mM glutamine, and 10 % (v/v) FBS, in standard culture conditions.

Sterile CoCrMo samples (n = 5 per condition) were transferred into separate wells of 12-well plates, and then SAOS-2 cells in 300 μL of culture medium were seeded onto each sample at a density of 10^4 cells/ cm^2. Afterwards, seeded samples were incubated in standard culture conditions for 3 and 7 days. At the end of the cell culture period, the supernatant was collected from each sample and assayed by means of the ALP activity colourimetric assay (BioVision Inc., USA) according to the manufacturer's instructions. Briefly, 20 μL of each supernatant were transferred to a 96-well plate, mixed with the ALP substrate (p-Nitrophenyl phosphate, pNPP) and incubated for 60 min at 25 °C. The absorbance at λ = 405 nm was next read using a Synergy H1 microplate reader. Absorbance values were referred to as an internal standard curve. Results from the ALP assay were then normalised to the ALP activity of CTRL samples. Data were expressed as mean ± standard deviation (SD). *2.5. Statistical analysis*

Statistical analysis was carried out by GraphPad version 6 (GraphPad Software, CA, USA). All data were initially analysed using D'Agostino and Pearson omnibus normality test. Comparisons among groups were performed by one-way ANOVA test followed by Tukey post-test compared the resulting data. Significance was retained when $p < 0.05$. Data are expressed as mean ± SD.

3. Results

3.1. Structural characterisation

The investigation of the crystalline structure of powder of TiO_2 dried at Room Temperature (RT, 25 °C) and after thermal treatment at 120 °C was carried out through XRD analysis. Fig. 1 shows powder X-ray diffraction patterns of two representative samples. The sharp peak occurring at 2θ = 25° corresponds to the (101) reflection, while the other characteristic peaks at 37°, 48° and 55° match different crystalline planes. The particle size of these two samples were estimated from the broadening of (101) anatase reflection using the Scherrer equation [30].

$$Dp = \frac{0.9\lambda}{\beta cs\theta}$$

where Dp, λ, θ, β are crystalline size, wavelength of X-ray, angle of diffraction (Bragg angle), and the line broadening at half the maximum intensity (FWHM). The average particle size was found to be 4 nm at RT, 5 nm at 120 °C.

3.2. Coating wettability and roughness

Surface wettability was evaluated by water contact angle (WCA) on the polished backside surface of samples. The WCA results of uncoated coated CoCrMo samples: one deposition in TiO_2 sol (1 layer); three depositions in TiO_2 sol (3 layers) are summarised in Fig. 2. The effects of sol–gel treatment on the resulting surface roughness were studied through the quantitative assessment of the following parameters: average roughness (Ra), root-mean-square roughness (Rq), skewness (Rsk) and kurtosis (Rk). The values of these parameters are reported in Table 1.

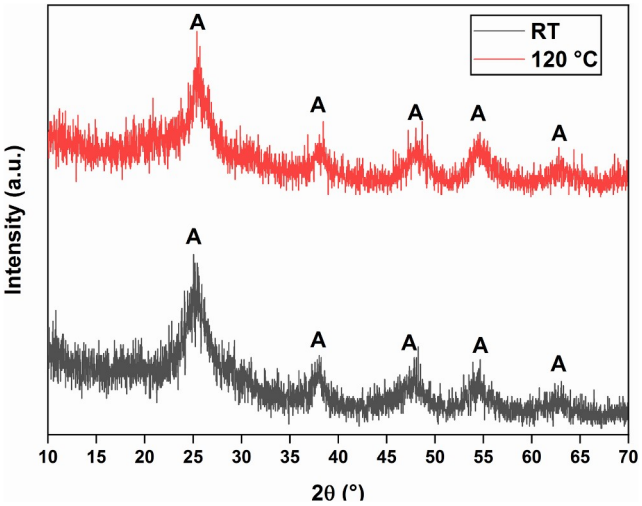

Fig. 1. Powder XRD patterns of TiO_2 at RT (grey line) and thermally treated at 120 °C (red line). The A peaks correspond to anatase (PDS 01-0562). samples (control, CTRL) and TiO_2-

3.3. Coating morphology and elements distribution

It was performed SEM-EDS analysis on the following CoCrMo disks: uncoated (control, CTRL), TiO_2-coated (plus Ag, one deposition TYPE I 1 layer; plus (Ag + Ga) one deposition TYPE III 1 layer), Fig. 3. The surface of CTRL sample had uniform roughness (Fig. 3**a**) due to sandblasting treatment with synthetic alumina. The SEM micrographs of TYPE I and TIPE III disks showed very similar characteristics to CTRL sample from a morphological poit of view (Fig. 3**b**, **c**), however a coating layer in the form of micro-flakes was observed at higher magnification (Fig. 3**c**). Concerning surface elemental composition, all EDS spectra revelead the elements of the alloy: Co, Cr and Mo. It was also found Al

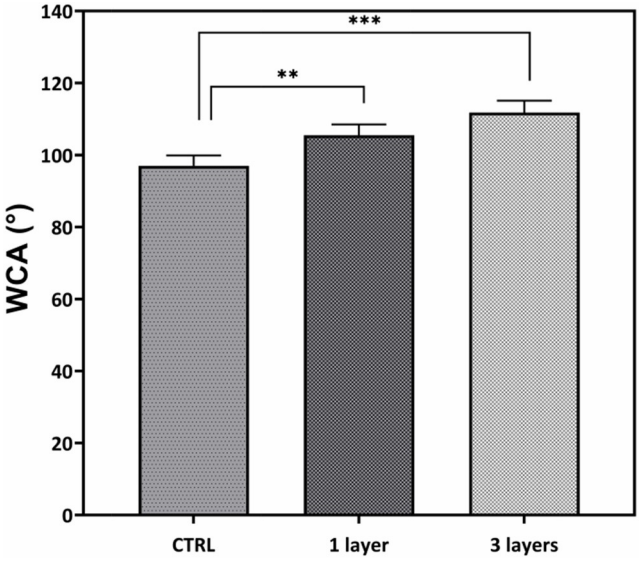

Fig. 2. WCA measurements of CTRL, 1 layer and 3 layers CoCrMo disks. Data are expressed as mean ± SD. (*p < 0.05, **p < 0.005, ***p < 0.0005).

Table 1
Surface roughness parameters (Ra, Rq, Rsk, Rk) for control (CTRL), 1 layer and 3 layers samples. Data are expressed as mean ± SD.

	Ra [μm]	Rq [μm]	Rsk	Rk
CTRL	3.30 (0.21)	4.18 (0.30)	− 0.037 (0.01)	3.13 (0.24)
1 layer	3.33 (0.20)	4.17 (0.24)	− 0.12 (0.15)	3.14 (0.058)
3 layers	3.04 (0.14)	3.83 (0.16)	− 0.15 (0.14)	3.16 (0.26)

because of the sandblasting treatment. EDS spectra of coated samples TYPE I and TYPE III pointed out the presence of Ti, Ag and Ga confirming the elemental composition of TiO_2 coating. Figs. 4 and 5 presented the GDOES patterns spectra of TiO_2-coated CoCrMo disks (plus Ga, one deposition TYPE II 1 layer; plus (Ag + Ga) one deposition TYPE III 1 layer), respectively. In both spectra, the concentration profile of Co, one of the main elements of CoCrMo alloy disk, gradually increases reaching a steady level. The concentration profile of Ti is higher than the other elements and it gradually decreases with depth, while the patterns of O, Ag e Ga display a trend similar to that of Ti indicating that the doping agents were embedded into the coating. The total amount of doping agents embedded in TiO_2 coatings was determined by ICP-OES analyses. Investigations were carried out on the following TiO_2-coated CoCrMo disks: plus Ga one deposition and three depositions TIPE II 1 layer, TYPE II 3 layers; plus (Ag + Ga) one deposition and three depositions TIPE III 1 layer, TYPE III 3 layers. Findings were summurized in Table 2. The amount of gallium and silver was found to increase with the number of layers obtained by dip coating.

3.4. In vitro biological characterisation of CoCrMo samples

The antibacterial properties of coated and uncoated CoCrMo-based materials against Gram-positive *S. aureus* bacteria (Fig. 6**a**) and Gram-negative *E. coli* bacteria (Fig. 6**b**) were assessed and compared. CoCrMo samples coated with TiO_2 doped with Ag (TYPE I) displayed a ≈99 % antibacterial efficiency against *S. aureus* as well as *E. coli* as compared to untreated control samples (CTRL; uncoated CoCrMo) ($p < 0.0001$). Similar results were obtained with CoCrMo samples coated with TiO_2 doped with both Ag and Ga ($p < 0.05$). Interestingly, CoCrMo samples coated with TiO_2 doped with Ga displayed a slight antibacterial activity against Gram-positive bacteria only, although of a less extent with respect to the Ag-containing coatings. Such results are in good agreement with literature data [31]. Overall, these results demonstrate that the antibacterial activity of the coating elements was mainly due to the presence of Ag, and agree with the literature [32–34].

On the other hand, the *in vitro* cytotoxicity of the most promising coatings was assessed, namely TYPE I and TYPE III. Indirect cytotoxicity tests were performed by challenging MG63 cells with the material extracts (harvested at 24 h and 72 h) to evaluate the cytotoxic effects of the material on cells. Results reported in Fig. 7 show that the viability of cells incubated with the material extracts (eluates) was comparable to those of cells cultured under standard conditions ($p > 0.05$ for all the conditions tested). Of note, these results demonstrate that the coatings were fully cytocompatible.

To further evaluate the potential osteoconductivity of the coatings, the ALP production and activity of cells cultured onto the samples were evaluated. Fig. 8 shows the results of the normalized ALP activity after 3 and 7 days of culture of SAOS-2 cells onto different samples. It was found that CoCrMo samples coated with TiO_2 doped with Ag (TYPE I) invariably induce higher ALP activity than the uncoated counterpart. More interestingly, the highest ALP activity was found in CoCrMo samples sol–gel coated with TiO_2 doped with Ag-Ga (TYPE III). Overall, such results suggest the potential osteoconductive properties of the coatings.

4. Discussion

In this study, the sol–gel dip-coating strategy was exploited to realise TiO_2 coatings on surfaces of CoCrMo samples in three main steps: 1) synthesis of TiO_2 sol by hydrolysis of the precursor TTIP with water in an acidic medium at RT; 2) dipping CoCrMo disks in TiO_2 sol; 3) thermal treatment at 120 °C for 3 h. XRD analyses were performed to study the crystalline structure of TiO_2 powders dried at RT and after thermal treatment of 120 °C. Both patterns of TiO_2 powders exhibit a sharp peak occurring at $2\theta = 25$ (Fig. 1**)**, which corresponds to the (101) reflection, while other characteristic peaks at $2\theta = 38, 48, 54, 55$ matching different crystalline planes. These peaks indicate the presence of the polycrystalline anatase structure of TiO_2. It is worthy of note that, among the three polymorphic forms of TiO_2, rutile is the most thermodynamically stable form of crystalline TiO_2, while anatase and brookite are metastable. Nevertheless, metastable anatase can be kinetically stabilised at lower temperatures [35], as here demonstrated. Furthermore, the XRD patterns of TiO_2 powders thermally treated at 120 °C for different times (respectively 3, 6 and 12 h) also confirmed the presence of the anatase crystalline phase (**Fig. S2**). The crystallite size values of the prepared TiO_2 nanopowders were estimated from XRD line broadening, using Scherrer's formula. In the present study, the particle size of the titania prepared by sol gel technique was found to be 5 nm at RT and 6 nm at 120 °C, respectively. It is worth poiting out that Scherrer's equation provides the average or the "apparent" crystallite size, since different factors such as microstrains, faulting, crystalline domain size, and domain size distribution affect peak broadening in diffraction pattern [36]. Therefore, the synthetic method here described enabled to preparation anatase TiO_2 nanoparticles at low temperature (RT, Fig. 1), avoiding: (i) non-aqueous alcohol media [37]; surfactant or polymers [38,39]; (iii) calcination steps [40]. The presence of either or both of these crystalline phases could affect the biocompatibility performance of the material. Notably, the anatase phase was found to induce *in vitro* bone-like apatite formation compared to the rutile phase [41].

Moreover, TiO_2 showed the ability to counteract different microorganisms, including bacteria [13]. In particular, the bactericidal activity of TiO_2 has been mostly ascribed to the photocatalytic activity of anatase, which is more photoactive than rutile and brookite [42,43].

It is well known that surface wettability plays an essential role in bacteria adhesion [44,45]. The degree to which a liquid can wet the surface is influenced by surface morphology and treatments. Static water contact angle (WCA) is the most commonly used technique to investigate the water wettability of surfaces. In this study, the sessile drop method was employed to determine the WCA: as shown in Fig. 2, all samples exhibited a hydrophobic behaviour; in particular, the greater the number of layers, the higher the hydrophobic behaviour of the CoCrMo surface. Although the debate concerning the efficacy of hydrophilic or hydrophobic surfaces for reducing bacterial adhesion is still ongoing, it has been proved that increasing the surface's hydrophobic features could imply the inhibition of bacteria adhesion [46]. Moreover, it has been demonstrated that CoCrMo samples, which have a more hydrophobic surface, displayed lower bacterial adhesion than the other materials (titanium alloys, commercially pure titanium (Cp-Ti) and stainless steel) [47]. Since the surface roughness plays an important role in bacterial adhesion [47–49] and implant osseointegration [50,51], the effects of the herein sol–gel surface treatment was evaluated on the resulting surface roughness through the quantitative assessment of the following parameters: average roughness (Ra), root-mean-square roughness (Rq), skewness (Rsk) and kurtosis (Rk). As shown in Table 1, Ra values of TiO_2-coated samples dipped one time (1 layer- samples) are very similar to control, whereas 3 layers samples (samples dipped three times in TiO_2 sol) exhibit slightly lower Ra values. Rq value parameter was determined because it provides information about surfaces with different profiles and distribution of surface texture. In our case, Rq values of control and 1 layer sample are very similar, lower for 3 layers samples than the control; thus, no very deep valley or very high peaks are present on surface. Generally, Rq shows a slightly (10–20 %) higher value than Ra, as seen in the current study; however, it was identified to be lower for 3 layers of coated samples. The two parameters Rsk and Rk are used to indicate the surface distribution's asymmetry and flatness, respectively: for a Gaussian distribution $Rsk = 0$ and $Rk = 3$ [52]. Each type of sample displays negative Rsk values. Rsk (the skewness index) measures the symmetry of the profile about the mean line, indicating how peaks and valleys are distributed throughout the surface. Negative Rsk means profiles with more valleys than asperities. Concerning Rk parameter (kurtosis index), which describes the sharpness of the probability density of the profile, all samples disclosed Rk values higher than 3, so relatively many high peaks and low valleys in the surface profile can be found. Thus, the values reported in Table 1 suggest that the sol–gel treatment does not significantly modify surface roughness.

The SEM micrographs and the corresponding Energy-dispersive X- ray (EDX) analysis of all investigated surfaces are reported in Fig. 3**.** Uncoated CoCrMo disks displayed an evident roughness due to the existence of micro-fractures. The EDS spectrum revealed the presence of Co, Cr, and Mo elements, which are the main element of alloy as well as Al, related to the alumina sandblasting media sometimes embedded in the surface (Fig. 3**a**).

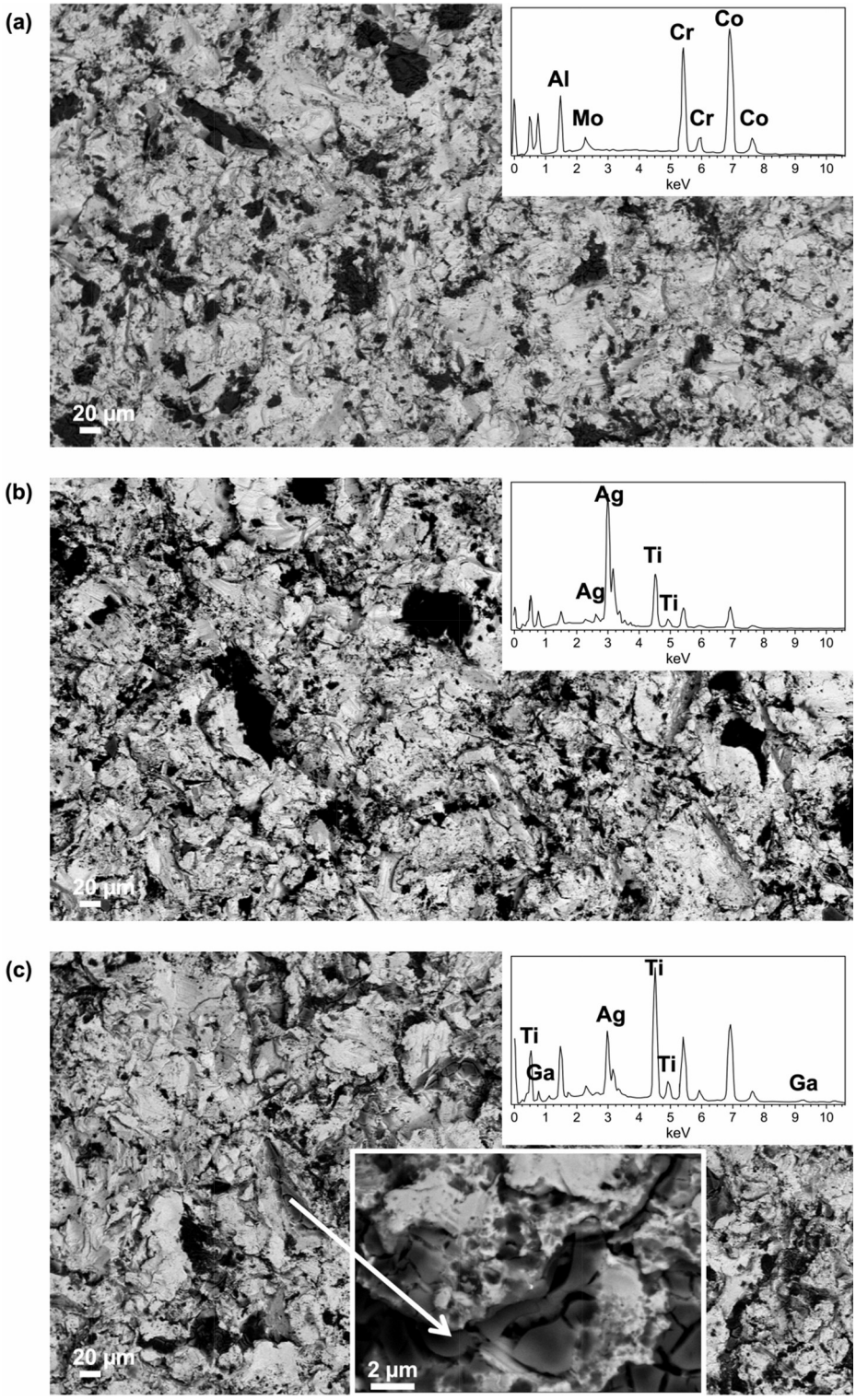

Fig. 3. SEM/EDS observation of: (a) CTRL sample (500X); (b) TYPE I 1 layer (500X); (c) TYPE III 1 layer (500X, insert 10.00kX).

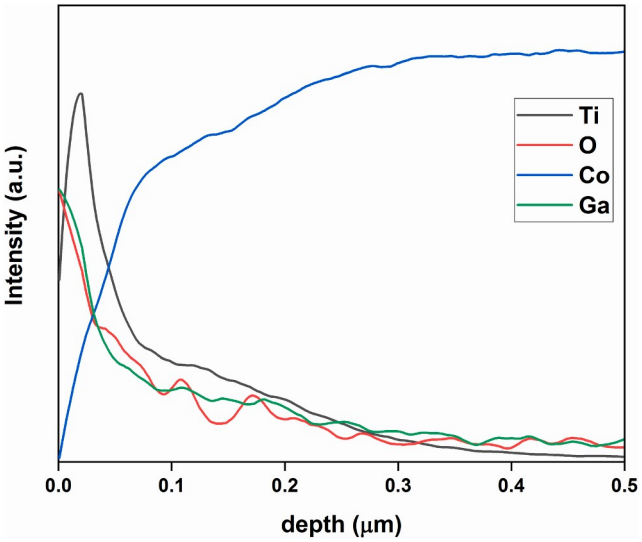

Fig. 4. GDOES profile of TYPE II 1 layer sample.

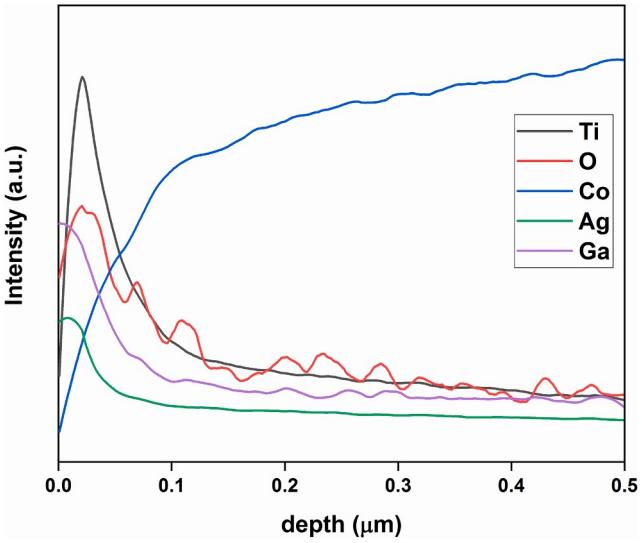

Fig. 5. GDOES profile of TYPE III 1 layer sample.

Table 2
ICP-OES results of total amount of Ga, Ag of TiO_2-coated CoCrMo disks: TYPE II (1 layer, 3 layers), TYPE III (1 layer, 3 layers).

	Ga [mg]	Ag [mg]	Area [cm^2]	Ga [$\mu g*cm^{-2}$]	Ag [$\mu g*cm^{-2}$]
TYPE II 1 layer	0.00338		1.54	2.19	
TYPE II 3 layers	0.00528		1.54	3.43	
TYPE III 1 layer	0.00255	0.00179	1.54	1.66	1.16
TYPE III 3 layers	0.00655	0.00319	1.54	4.25	2.07

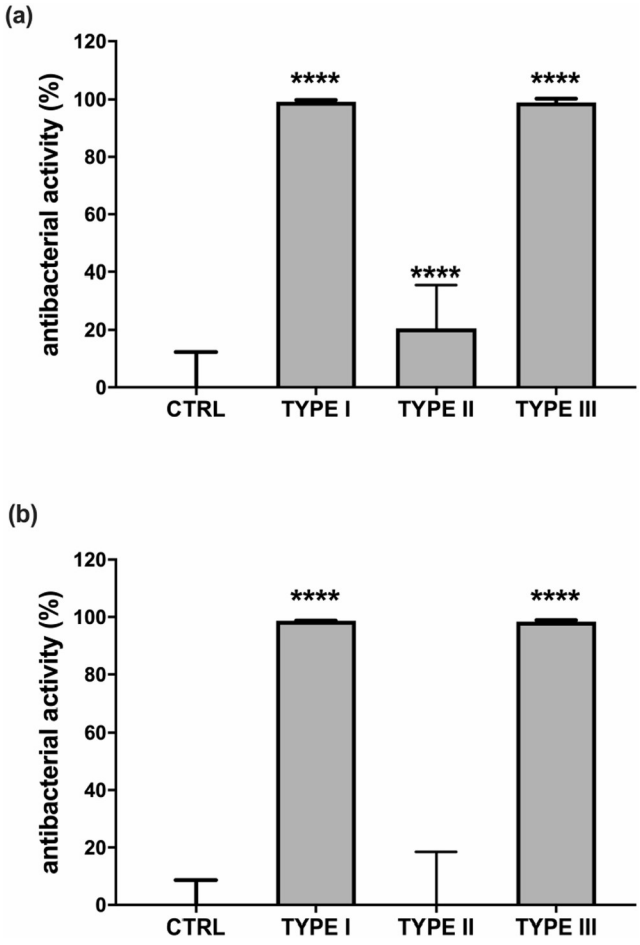

Fig. 6. Antibacterial activity of material extracts against (a) Gram-positive (*S. aureus*) and (b) Gram-negative (*E. coli*) bacterial strains. Bacteria were inoculated onto CoCrMo-based samples. After a 24 h-incubation the OD_{600nm} was read. Data are expressed as mean ± SD (**** $p < 0.0001$ vs CTRL).

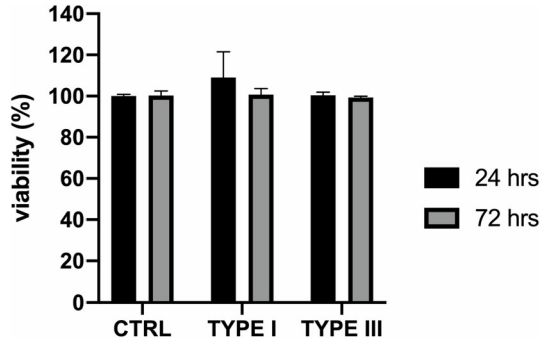

Fig. 7. Indirect cytotoxicity tests of material extracts on MG63 cell line. CoCrMo samples were incubated with standard culture medium, and material extracts (eluates) were collected 24 h and 72 h post-incubation.

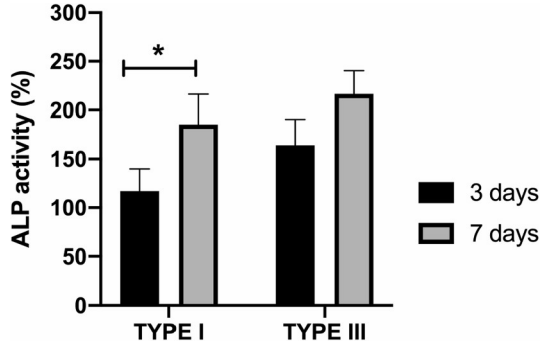

Fig. 8. Evaluation of osteodifferentiation potential of different coatings. SAOS- 2 cells were cultured onto different samples, and at day 3 and 7 the alkaline phosphatase (ALP) activity was evaluated. ALP data were normalised to the ALP activity of CTRL samples. Results are expressed as means ± SD (*p < 0.05).

Even if the surface morphology of TiO_2-coated disk seemed to be very similar to uncoated sample (Fig. 3**b**), the EDS analysis not only showed the presence of Ti, confirming surface modification, but also corroborated the incorporation of Ag (Fig. 3**b**). Similarly, TiO_2- coated disk plus (Ag + Ga) exhibited a homogeneous coating (Fig. 3**c**). At higher magnification (Fig. 3**c insert**), it can be seen the coating layer in the form of micro-flakes, that may have been attributed to the shrink of TiO_2 coatings during the heat treatment due to low cohesive strength in the titanium dioxide coating and low adhesion strength between the coating and the substrate surface. The EDS elemental analysis revealed that the coating was mainly composed by Ti and Ag as well as Ga has been incorporated inside it (Fig. 3**c**). Furthermore, SEM micrograph of sample coated by three layers even show a uniform coating with micro- flakes (Fig. S3**a**). To test early stability, samples were rinsed in ethanol three times, then SEM and EDS analyses were performed. The coating seemed to preserve its structure and morphology (Fig. S3**b**), with Ti, Ag and Ga element still present at the surface. GDOES profiles (Fig. 4 and Fig. 5) not only proved the presence of TiO_2 coatings on CoCrMo disks, but also confirmed the inclusion of doping agents into coatings. Furthermore, it was possible to estimate the coating thickness: 50 nm after one layer deposition (**Fig. S4**) and 180 nm for sample coated by three layers (**Fig. S5**). These values indicate that increasing the number of depositions increases the coating thickness.

Although CoCrMo-based alloys have been widely used as implant materials in orthopaedics, issues related to the infections occurring after implantation may lead to the undesired failure of the implant [53]. Hence, the development of functional antibacterial materials can be an effective method for preventing the infection-related failure of metal implants. It is generally accepted that metal ions, such as Ag, Ga, and Cu [29] and their oxides [54] have an interesting ability to inhibit and control different microorganisms proliferation, including bacteria [13]. Therefore, surface modification and coating treatments can be exploited to incorporate such elements to provide antibacterial properties. Coatings containing antibacterial ions for implantable devices should effectively exert antimicrobial activity and minimize toxicity to human cells. Silver nitrate is a common source of silver ions, whose impact on bacteria and human cells is well known [55,56]. Recently, the ability of gallium nitrate to prevent the formation of biofilm and to eradicate was already assessed [23,24]. On the basis of previous studies [57,58], MIC (minimal inhibitory concentration) of silver and gallium has been considered to prepare effective antibacterial coatings. After verifying the incorporation of gallium and silver, ICP-OES analyses were carried out to determine the total amount of the doping agents in the sol–gel coating. The amount of gallium and silver was found to increase with the number of layers obtained by dip coating (Table 2). Notably, such amount of antibacterial agents should ensure antimicrobial activity while maintaining biocompatibility [59,60]. Overall, these biological characterisation results suggest that CoCrMo samples sol–gel coated with TiO_2 doped with Ag-Ga are suitable for orthopaedic implant applications.

Surface modification of implants represents a straightforward strategy to make the surfaces of biomedical devices antimicrobial. Several studies have reported the development of implant surface coating enabling the damage of the bacterial membrane or wall or were characterised by anti-adhesive properties. They inhibited bacterial adhesion in the first place [16,17]. In this work, a TiO_2 sol–gel coating doped with Ag and Ga was developed to provide CoCrMo-based materials with outstanding antimicrobial properties against Gram-positive *S. aureus* and Gram-negative *E. coli* bacteria (Fig. 6). In this phase, a single layer coating was preferred to a multilayer due to the prospect of industrial applicability: although easy to obtain in the laboratory, a multilayer coating can make industrial processing more complicated without providing substantial benefits. Our results demonstrate that the considered coatings were fully cytocompatible (Fig. 7) with marked osteoconductive potential (Fig. 8), as demonstrated by ALP activity, an early-stage biomarker associated with bone formation [53]. These data are in good agreement with published literature [61] and suggests that the presence of Ga positively promote the osteogenic potential of the newly developed coatings [61].

It is important to note that further biological investigations are necessary to better evaluate the anti-biofilm activity of coatings and to deeply assess the potential ability to enhance osteo-integration. Another limit of the present study is related to the assessment of adhesion and mechanical stability of such coating onto CoCrMo alloy. Nevertheless, these preliminarily results suggest that this can be a promising strategy to realize anti-infective coatings to prevent microbial infections on orthopaedic implants. Furthermore, this approach could be also useful to cover other implant materials such as titanium alloys, widely employed in orthopaedic field.

5. Conclusions

In the current study, titanium dioxide coatings doped with silver and gallium were successfully obtained by sol–gel dipping technique onto the surface of CoCrMo samples. The obtained coatings provided promising antimicrobial action against *S. aureus* and *E. coli* pathogens with no cytotoxic effect as well as osteo differentiation potential. Based on these preliminary *in vitro* studies, this new class of coatings could become an important tool for orthopaedic implantology by reducing bacterial colonization, while maintaining biocompatibility and even improving osteogenic differentiation. These results constitute a valid starting point to develop a new class of coatings for improving CoCrMo orthopaedic implant performance.

CRediT authorship contribution statement

Agnese D'Agostino: Methodology, Investigation, Data curation, Writing – original draft, Writing – review & editing. **Michele Bertolini:** Methodology, Investigation. **Nina Bono:** Investigation, Data curation, Writing – review & editing. **Matteo Pavarini:** Methodology, Investigation. **Paolo Tarsini:** Methodology, Investigation. **Gabriele Candiani:** Investigation, Writing – review & editing. **Luigi De Nardo:** Writing – review & editing. **Roberto Chiesa:** Writing – review & editing, Supervision.

Declaration of Competing Interest

The authors declare that they have no known competing financial interests or personal relationships that could have appeared to influence the work reported in this paper.

Data availability

Data will be made available on request.

Acknowledgement

Authors would like to acknowledge project PRIN “Multiple Advanced Materials Manufactured by Additive Technologies – PRIN 2017 - prot. 20179SWLKA” and project FESR 2014–2020 ARS01_01205 ‘CustOmmadeaNTibacterical/bioActive/bioCoated Prostheses’ for the economic support.

References

[1] A.M. Ribeiro, T.H.S. Flores-Sahagun, R.C. Paredes, A perspective on molybdenum biocompatibility and antimicrobial activity for applications in implants, J. Mater. Sci. 51 (2016) 2806–2816.

[2] European Parlament, Council of the European Union, Regulation (EU) 2017/745 of the European Parliament and of the Council of 5 April 2017 on medical devices, Off. J. Eur. Union. 60 (2017) 2–175. <http://data.europa.eu/eli/reg/2017/745/ 2020-04-24>.

[3] G. Eichenbaum, J.T. Wilsey, G. Fessel, Q.-Q. Qiu, L. Perkins, P. Hasgall, A. Monnot, S.L. More, N. Egnot, J. Sague, An integrated benefit-risk assessment of cobalt- containing alloys used in medical devices: implications for regulatory requirements in the European Union, Regul. Toxicol. Pharmacol. 125 (2021) 105004.

[4] M. Kovochich, A. Monnot, D.G. Kougias, S.L. More, J.T. Wilsey, Q.-Q. Qiu, L.E. L. Perkins, P. Hasgall, M. Taneja, E.E. Reverdy, Carcinogenic hazard assessment of cobalt-containing alloys in medical devices: review of in vivo studies, Regul. Toxicol. Pharmacol. 122 (2021) 104910.

[5] S. Zhang, C.E. Holy, G. Eichenbaum, L.E. Perkins, P. Hasgall, L.B. Katz, J.R. Brown, L. Orlandini, G. Fessel, B. Nasseri-Aghbosh, Carcinogenic assessment of cobalt- containing alloys in medical devices or cobalt in occupational settings: a systematic review and meta-analysis of overall cancer risk from published epidemiologic studies, Regul. Toxicol. Pharmacol. 125 (2021) 104987.

[6] B.H. Kapadia, R.A. Berg, J.A. Daley, J. Fritz, A. Bhave, M.A. Mont, Periprosthetic joint infection, Lancet. 387 (2016) 386–394, https://doi.org/10.1016/S0140-6736 (14)61798-0.

[7] C. Renata, D. Campoccia, P. Speziale, L. Montanaro, J. William, Biomaterials Bio fi lm formation in Staphylococcus implant infections. A review of molecular mechanisms and implications for bio fi lm-resistant materials, Biomaterials. 33 (2012) 5967–5982.

[8] J.P. Guggenbichler, O. Assadian, M. Boeswald, A. Kramer, Incidence and clinical implication of nosocomial infections associated with implantable biomaterials–catheters, ventilator-associated pneumonia, urinary tract infections, GMS Krankenhhyg. Interdiszip. 6 (2011).

[9] S. Corvec, M.E. Portillo, B.M. Pasticci, O. Borens, A. Trampuz, Epidemiology and new developments in the diagnosis of prosthetic joint infection, Int. J. Artif. Organs. 35 (2012) 923–934.

[10] D. Campoccia, L. Montanaro, C.R. Arciola, A review of the biomaterials technologies for infection-resistant surfaces, Biomaterials. 34 (2013) 8533–8554, https://doi.org/10.1016/j.biomaterials.2013.07.089.

[11] E. Tranquillo, F. Bollino, Surface modifications for implants lifetime extension: an overview of sol-gel coatings, Coatings. 10 (2020) 589, https://doi.org/10.3390/coatings10060589.

[12] A. Duran, Y. al Castro, M. Aparicio, A. Conde, J.J. De Damborenea,, Protection and ´ surface modification of metals with sol–gel coatings, Int. Mater. Rev. 52 (2007) 175–192, https://doi.org/10.1179/174328007X160263.

[13] S. Jafari, B. Mahyad, H. Hashemzadeh, S. Janfaza, T. Gholikhani, L. Tayebi, Biomedical applications of tio2 nanostructures: recent advances, Int. J. Nanomed. 15 (2020) 3447.

[14] Z.F. Yin, L. Wu, H.G. Yang, Y.H. Su, Recent progress in biomedical applications of titanium dioxide, Phys. Chem. Chem. Phys. 15 (2013) 4844–4858, https://doi.org/10.1039/C3CP43938K.

[15] T. Lopez, E. Ortiz, M. Alvarez, J. Navarrete, J.A. Odriozola, F. Martinez-Ortega, E. A. Paez-Mozo, P. Escobar, K.A. Espinoza, I.A. Rivero, Study of the stabilization of ´ zinc phthalocyanine in sol-gel TiO2 for photodynamic therapy applications, Nanomed. Nanotechnol. Biol. Med. 6 (2010) 777–785, https://doi.org/10.1016/j. nano.2010.04.007.

[16] C.L. Romano, S. Scarponi, E. Gallazzi, D. Roma` no, L. Drago, Antibacterial coating` of implants in orthopaedics and trauma: a classification proposal in an evolving panorama, J. Orthop. Surg. Res. 10 (2015) 1–11.

[17] C. Mas-Moruno, B. Su, M.J. Dalby, and Nanotopographies: Toward Cell Instructive and Antibacterial Implants. Advanced Healthcare Materials, 8 (1),[1801103]., Adv. Healthc. Mater. 8 (n.d.) 1801103.

[18] D.S. Ahmed, M.K.A. Mohammed, M.R. Mohammad, Sol–gel synthesis of Ag-doped titania-coated carbon nanotubes and study their biomedical applications, Chem. Pap. 74 (2020) 197–208.

[19] L. Mai, D. Wang, S. Zhang, Y. Xie, C. Huang, Z. Zhang, Synthesis and bactericidal ability of Ag/TiO2 composite films deposited on titanium plate, Appl. Surf. Sci. 257 (2010) 974–978, https://doi.org/10.1016/j.apsusc.2010.08.003.

[20] E. Jager, J. Schmidt, A. Pfuch, S. Spange, O. Beier, N. ¨ Jager, O. Jantschner,¨ R. Daniel, C. Mitterer, Antibacterial silicon oxide thin films doped with zinc and copper grown by atmospheric pressure plasma chemical vapor deposition, Nanomaterials. 9 (2019) 255.

[21] B. Pietrzyk, K. Porębska, W. Jakubowski, S. Miszczak, Antibacterial properties of Zn doped hydrophobic SiO2 coatings produced by sol-gel method, Coatings 9 (2019) 362, https://doi.org/10.3390/coatings9060362.

[22] J. Dong, D. Fang, L. Zhang, Q. Shan, Y. Huang, Gallium-doped titania nanotubes elicit anti-bacterial efficacy in vivo against Escherichia coli and Staphylococcus aureus biofilm, Materialia. 5 (2019) 100209, https://doi.org/10.1016/j. mtla.2019.100209.

[23] A. Cochis, B. Azzimonti, C. Della Valle, R. Chiesa, C.R. Arciola, L. Rimondini, Biofilm formation on titanium implants counteracted by grafting gallium and silver ions, J. Biomed. Mater. Res. Part A. 103 (2015) 1176–1187, https://doi.org/ 10.1002/jbm.a.35270.

[24] A. D’Agostino, F. Tana, A. Ettorre, M. Pavarini, A. Serafini, A. Cochis, A.C. Scalia, L. Rimondini, E. De Giglio, S. Cometa, Mesoporous zirconia surfaces with anti- biofilm properties for dental implants, Biomed. Mater. 16 (2021) 45016.

[25] T. Schmidt-Braekling, A. Streitbuerger, G. Gosheger, F. Boettner, M. Nottrott, H. Ahrens, R. Dieckmann, W. Guder, D. Andreou, G. Hauschild, Silver-coated megaprostheses: review of the literature, Eur. J. Orthop. Surg. Traumatol. 27 (2017) 483–489, https://doi.org/10.1007/s00590-017-1933-9.

[26] R. Kuehl, P.S. Brunetto, A.-K. Woischnig, M. Varisco, Z. Rajacic, J. Vosbeck, L. Terracciano, K.M. Fromm, N. Khanna, Preventing implant-associated infections by silver coating, Antimicrob. Agents Chemother. 60 (2016) 2467–2475.

[27] C. Marambio-Jones, E.M.V. Hoek, A review of the antibacterial effects of silver nanomaterials and potential implications for human health and the environment, J. Nanoparticle Res. 12 (2010) 1531–1551.

[28] A. Cochis, B. Azzimonti, R. Chiesa, L. Rimondini, M. Gasik, Metallurgical gallium additions to titanium alloys demonstrate a strong time-increasing antibacterial activity without any cellular toxicity, ACS Biomater. Sci. Eng. 5 (2019) 2815–2820.

[29] L. Bonetti, L. Altomare, N. Bono, E. Panno, C.E. Campiglio, L. Draghi, G. Candiani, S. Fare, A.R. Boccaccini, L. De Nardo, Electrophoretic processing of chitosan based` composite scaffolds with Nb-doped bioactive glass for bone tissue regeneration, J. Mater. Sci. Mater. Med. 31 (2020) 1–12.

[30] B.D. Cullity, S.R. Stock, Elements of X-Ray diffraction, addisonwesley, reading, MA Google Sch. (1978).

[31] F. Minandri, C. Bonchi, E. Frangipani, F. Imperi, P. Visca, Promises and failures of gallium as an antibacterial agent, Future Microbiol. 9 (2014) 379–397, https://doi.org/10.2217/fmb.14.3.

[32] N. Kircheva, T. Dudev, Gallium as an antibacterial agent: a DFT/SMD study of the Ga3+/Fe3+ competition for binding bacterial siderophores, Inorg. Chem. 59 (2020) 6242–6254.

[33] E. Albert, P.-A. Albouy, A. Ayral, P. Basa, G. Csík, N. Nagy, S. Roualdes, V. Rouessac, G. Safran, A. Suhajda, Antibacterial properties of Ag–TiO 2 composite sol–gel coatings, RSC Adv. 5 (2015) 59070–59081.

[34] H. Zhang, G. Chen, Potent antibacterial activities of Ag/TiO2 nanocomposite powders synthesized by a one-pot sol− gel method, Environ. Sci. Technol. 43 (2009) 2905–2910.

[35] D.A.H. Hanaor, C.C. Sorrell, Review of the anatase to rutile phase transformation, J. Mater. Sci. 46 (2011) 855–874.

[36] A. Weibel, R. Bouchet, F. Boulc’, P. Knauth,, The big problem of small particles: a comparison of methods for determination of particle size in nanocrystalline anatase powders, Chem. Mater. 17 (2005) 2378–2385.

[37] E. Burunkaya, M. Akarsu, H.E. Çamurlu, O. Kesmez, Z. Ye ¨ s¸il, M. Asiltürk, E. Arpaç, Production of stable hydrosols of crystalline TiO2 nanoparticles synthesized at relatively low temperatures in diverse media, Appl. Surf. Sci. 265 (2013) 317–323.

[38] D.L. Liao, B.Q. Liao, Shape, size and photocatalytic activity control of TiO2 nanoparticles with surfactants, J. Photochem. Photobiol. A Chem. 187 (2007) 363–369.

[39] Y. Li, Z. Qin, H. Guo, H. Yang, G. Zhang, S. Ji, T. Zeng, Low-temperature synthesis of anatase TiO2 nanoparticles with tunable surface charges for enhancing photocatalytic activity, PLoS One 9 (2014) e114638.
[40] F. Bosc, A. Ayral, P.-A. Albouy, C. Guizard, A simple route for low-temperature synthesis of mesoporous and nanocrystalline anatase thin films, Chem. Mater. 15 (2003) 2463–2468.
[41] V. Sollazzo, A. Palmieri, F. Pezzetti, A. Scarano, M. Martinelli, L. Scapoli, L. Massari, G. Brunelli, E. Caramelli, F. Carinci, Genetic effect of anatase on osteoblast-like cells, J. Biomed. Mater. Res. - Part B Appl. Biomater. 85 (2008) 29–36, https://doi.org/10.1002/jbm.b.30912.
[42] C. Liao, Y. Li, S.C. Tjong, Visible-light active titanium dioxide nanomaterials with bactericidal properties, Nanomaterials 10 (2020), https://doi.org/10.3390/ nano10010124.
[43] L. Visai, L. de Nardo, C. Punta, L. Melone, A. Cigada, M. Imbriani, C.R. Arciola, Titanium oxide antibacterial surfaces in biomedical devices, Int. J. Artif. Organs. 34 (2011) 929–946, https://doi.org/10.5301/ijao.5000050.
[44] K. Liu, X. Yao, L. Jiang, Recent developments in bio-inspired special wettability, Chem. Soc. Rev. 39 (2010) 3240–3255.
[45] W. Song, J.F. Mano, Interactions between cells or proteins and surfaces exhibiting extreme wettabilities, Soft Matter. 9 (2013) 2985–2999, https://doi.org/10.1039/ c3sm27739a.
[46] G. Wang, D. Weng, C. Chen, L. Chen, J. Wang, Influence of TiO2 nanostructure size and surface modification on surface wettability and bacterial adhesion, Colloids Interface Sci. Commun. 34 (2020) 100220, https://doi.org/10.1016/j. colcom.2019.100220.
[47] I. Yoda, H. Koseki, M. Tomita, T. Shida, H. Horiuchi, H. Sakoda, M. Osaki, Effect of surface roughness of biomaterials on Staphylococcus epidermidis adhesion, BMC Microbiol. 14 (2014) 1–7.
[48] T.R. Scheuerman, A.K. Camper, M.A. Hamilton, Effects of substratum topography on bacterial adhesion, J. Colloid Interface Sci. 208 (1998) 23–33.
[49] W. Teughels, N. Van Assche, I. Sliepen, M. Quirynen, Effect of material characteristics and/or surface topography on biofilm development, Clin. Oral Implants Res. 17 (2006) 68–81.
[50] J. Tavakoli, M.E. Khosroshahi, Surface morphology characterization of laser- induced titanium implants: lesson to enhance osseointegration process, Biomed, Eng. Lett. 8 (2018) 249–257.
[51] B.A.J.A. Van Oirschot, R.M. Eman, P. Habibovic, S.C.G. Leeuwenburgh, Z. Tahmasebi, H. Weinans, J. Alblas, G.J. Meijer, J.A. Jansen, J.J.J.P. Van Den Beucken, Osteophilic properties of bone implant surface modifications in a cassette model on a decorticated goat spinal transverse process, Acta Biomater. 37 (2016) 195–205.
[52] N. Tayebi, A.A. Polycarpou, Modeling the effect of skewness and kurtosis on the static friction coefficient of rough surfaces, Tribol. Int. 37 (2004) 491–505, https:// doi.org/10.1016/j.triboint.2003.11.010.
[53] J. Tang, H. Li, M. Guo, Z. Zhao, H. Liu, Y. Ren, J. Wang, X. Cui, Y. Shen, H. Jin, Enhanced spreading, migration and osteodifferentiation of HBMSCs on macroporous CS-Ta–A biocompatible macroporous coating for hard tissue repair, Mater. Sci. Eng. C. 129 (2021) 112411.
[54] G.V. Vimbela, S.M. Ngo, C. Fraze, L. Yang, D.A. Stout, Antibacterial properties and toxicity from metallic nanomaterials, Int. J. Nanomedicine. 12 (2017) 3941.
[55] E. Hidalgo, C. Domınguez, Study of cytotoxicity mechanisms of silver nitrate in human dermal fibroblasts, Toxicol. Lett. 98 (1998) 169–179.
[56] A. Hamad, K.S. Khashan, A. Hadi, Silver nanoparticles and silver ions as potential antibacterial agents, J. Inorg. Organomet. Polym. Mater. 1–18 (2020).
[57] A.B. Kelson, M. Carnevali, V. Truong-Le, Gallium-based anti-infectives: targeting microbial iron-uptake mechanisms, Curr. Opin. Pharmacol. 13 (2013) 707–716. [58] T. Hrkac, C. Rohl, R. Podschun, V. Zaporojtchenko, T. Strunskus, ¨ H. Papavlassopoulos, D. Garbe-Schonberg, F. Faupel, Huge increase of therapeutic ¨ window at a bioactive silver/titania nanocomposite coating surface compared to solution, Mater. Sci. Eng. C. 33 (2013) 2367–2375, https://doi.org/10.1016/j. msec.2013.01.069.
[59] M. Bosetti, A. Masse, E. Tobin, M. Cannas, Silver coated materials for external ` fixation devices: In vitro biocompatibility and genotoxicity, Biomaterials. 23 (2002) 887–892, https://doi.org/10.1016/S0142-9612(01)00198-3.
[60] C. Bonchi, F. Imperi, F. Minandri, P. Visca, E. Frangipani, Repurposing of gallium- based drugs for antibacterial therapy, BioFactors. 40 (2014) 303–312, https://doi. org/10.1002/biof.1159.
[61] M. Yu, Y. Wang, Y. Zhang, D. Cui, G. Gu, D. Zhao, Gallium ions promote osteoinduction of human and mouse osteoblasts via the TRPM7/Akt signaling pathway, Mol. Med. Rep. 22 (2020) 2741–2752.